JOURNAL OF MATERIALS SCIENCE 21 (1986) 1747–1757

Tracer diffusion studies in NiO bicrystals and polycrystals

A. ATKINSON, D. P. MOON, D. W. SMART, R. I. TAYLOR
Materials Development Division, AERE Harwell, Didcot, Oxon OX11 ORA, UK

The tracer self-diffusion of nickel in two NiO bicrystals and a polycrystalline specimen at 700° C has been studied using sectioning and autoradiography. The two bicrystal boundaries were ⟨1 1 0⟩ symmetrical tilt boundaries with misorientations of 39.5° and 99.5°, respectively. After diffusion measurements the bicrystals were fractured and the boundaries studied by a variety of surface analysis techniques. The tracer penetration profiles were analysed in terms of lattice diffusion and diffusion along low angle boundaries composed of dislocation arrays introduced by mechanical polishing. The coefficients for lattice and low angle boundary diffusion are in acceptable agreement with previous determinations. Diffusion along high angle boundaries could not be detected by profiling, but could be detected by autoradiography in some boundaries after annealing at high temperature (1400° C) before the diffusion anneal. Autoradiography also revealed that the boundary diffusion was not homogeneous and was sensitive to both thermal history and boundary geometry. The bicrystal boundaries were found to be extensively contaminated by calcium and silicon compounds. It is concluded that high angle boundary diffusion in the present experiments is dominated by these impurities and their distribution. The implications for other measurements of grain boundary properties are discussed and the need for chemical characterization of the actual boundaries used in measurements of boundary properties is emphasized.

1. Introduction

Diffusion along grain boundaries is a particularly important pathway for material transport in oxides. It is known, or suspected, to control many important processes (such as sintering, creep, metal oxidation) even at unexpectedly high temperatures. For example, it has been shown that the oxidation of nickel to NiO is controlled by the outward diffusion of nickel along grain boundaries in the NiO film at temperatures below about 1100° C [1]. The general level of understanding of diffusion in oxide grain boundaries is not very good and even reliable data are not abundant [2]. NiO is the oxide for which most data do exist and for which there are also good data available for lattice diffusion.

The data for diffusion of nickel and oxygen in the lattice and of nickel along grain boundaries are summarized in Fig. 1. In the case of grain boundaries the experiments usually give the product of the boundary diffusion coefficient, D', and the boundary width, δ. There is good experimental evidence for δ being approximately 1 nm [3]. Therefore the scales for D and $D'\delta$ in Fig. 1 have been offset so that if $\delta = 1$ nm, D' can be compared directly with lattice diffusion, D. It has also been established that diffusion of nickel through the NiO lattice is by a vacancy mechanism [4, 5] which results in a characteristic dependence of D on oxygen activity in the gas. A similar dependence has also been observed for $D'\delta$ for nickel in both high- and low-angle grain boundaries [3, 6]. This strongly suggests that grain-boundary diffusion also involves a point defect analogous to a lattice vacancy and that the grain-boundary diffusion data for NiO are characteristic of the pure, non-stoichiometric, oxide.

A far better insight into the atomic mechanism of grain-boundary diffusion has come from computer simulation both in metals [7] and in oxides [8]. These simulations support the concept of localized point defects in the boundaries and enable the energies which control their concentrations and mobilities to be estimated. A necessary consequence of the computational constraints is that only boundaries of relatively high symmetry can be tackled. For NiO, however, self-diffusion data only exist for random low angle boundaries, formed by the rearrangement of dislocations in single crystals, and random high angle boundaries, in a polycrystalline NiO film grown by the oxidation of nickel. Therefore, in order to make detailed comparison between theory and experiment it is preferable for experiments to be done on single boundaries of known and simple misorientation.

Such experiments have been reported for metals [9] with varying degrees of success. In silver, nickel and lead there is reasonable correspondence between grain-boundary diffusion measured in polycrystalline specimens and in single high angle boundaries of simple misorientation [10]. Attempts to study grain-boundary diffusion as a function of misorientation have not been unequivocal and agreement between different workers is poor. Only one misorientation has so far been generally recognized as having low

0022–2461/86 $03.00 + .12

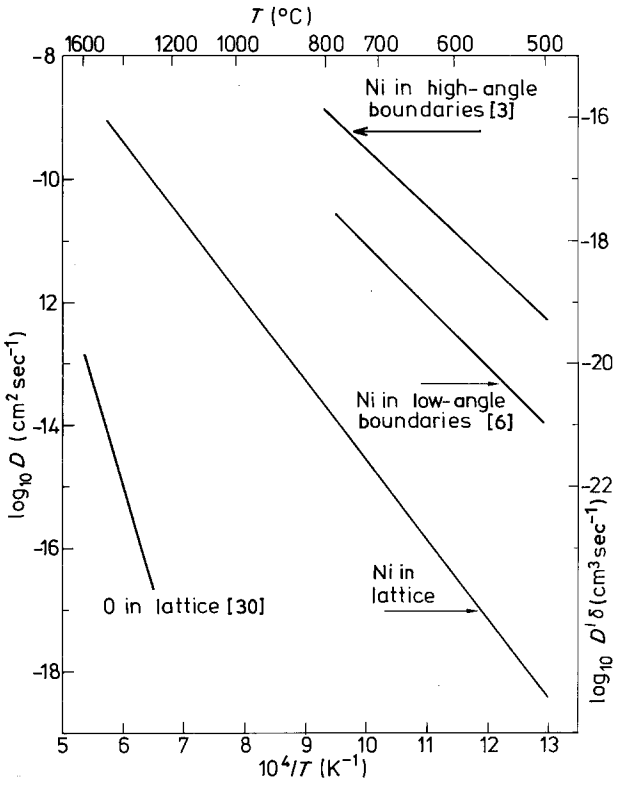

Figure 1 Summary of previous determinations of diffusion parameters for NiO. The nickel data are at an oxygen activity of unity and the oxygen data at an oxygen activity of 0.2. The scale for $D'\delta$ (grain boundary diffusion) has been offset so that if $\delta = 1$ nm D' is given directly on the scale for D [3, 6, 30].

diffusitivity and that is the $\Sigma = 3, \langle 1\,1\,0\rangle$ symmetrical tilt boundary ($\theta = 70.5°$), which is a coherent twin boundary.

Diffusion experiments using bicrystal specimens (i.e. containing a single boundary) of oxides have also been attempted in the past. Wuensch and Vasilos [11] measured nickel diffusion in MgO bicrystals and polycrystals. The bicrystals were either "natural", of uncontrolled misorientation, or "synthetic" (produced by hot pressing) and of controlled misorientation. Microprobe analysis was used to detect grain-boundary diffusion in the bicrystals at 1200° C, but no estimates of $D'\delta$ were made from these data. McKenzie *et al.* [12] also used "natural" MgO bicrystals for studies of oxygen diffusion. Grain-boundary diffusion was detected by autoradiography following proton activation of ^{18}O tracer and estimates of $D'\delta$ were obtained ($\sim 10^{-15}$ cm^3 sec^{-1} at 1700° C). More recently Osenbach and Stubican [13] studied ^{51}Cr diffusion in MgO and Cr-doped MgO bicrystals of known misorientation. Grain boundary diffusion was detected and characterized by serial sectioning. The results confirmed qualitatively the expected anisotropy of diffusion and the increase in $D'\delta$ with increasing misorientation, θ, in low angle tilt boundaries. They observed that $D'\delta$ increased as the Cr doping level increased, which is consistent with a vacancy mechanism of diffusion. Hirota and Komatsu [14] studied nickel diffusion in Al_2O_3 bicrystals fabricated by pressure-less sintering. Grain-boundary diffusion was observed by microprobe analysis and values for $D'\delta$ were estimated. Finally, Chen and Peterson [15] studied ^{57}Co diffusion in NiO bicrystals and large-grained polycrystalline specimens. Serial sectioning was used to detect grain-boundary diffusion and measure $D'\delta$. (These results are not in good agreement with those of Atkinson and Taylor [16] measured in polycrystalline films grown by oxidation of nickel.) On the other hand, Revcolevschi *et al.* [17] have also studied cobalt diffusion in NiO bicrystals and were unable to detect fast grain-boundary diffusion under any conditions.

There are several general comments to be made concerning this earlier work on single boundaries. First, only one of the measurements (oxygen in MgO) is of self-diffusion (although cobalt in NiO is probably a good approximation to self-diffusion). Second, the defect concentrations in pure MgO and Al_2O_3 are expected to be so small that the transport properties of real samples of these oxides are always controlled by foreign atoms. An oxide such as NiO is preferable because it is known to have a much larger and controllable concentration of lattice point defects. Third, and perhaps most important, in no case have the boundaries been characterized in terms of chemical composition. The aim of the work described here was to measure grain-boundary diffusion in individual boundaries of NiO having a known, simple misorientation and to characterize the chemistry of the same grain boundaries.

2. Experiments

2.1. Diffusion specimens

The specimens used in the diffusion anneals were two NiO bicrystals and one large-grained polycrystalline specimen. They were provided by A. Revolevschi and F. Barbier (Université Paris Sud, Orsay, France) and had been grown by flame fusion from oriented seeds (for the two bicrystals) using "Specpure" grade NiO powder. The two bicrystal specimens each contained a single grain boundary formed by a symmetrical tilt about the $\langle 1\,1\,0\rangle$ direction. In bicrystal 1 the tilt angle was 39.5° and in bicrystal 2 it was 99.5°. The specimens were in the form of discs approximately 10 mm diameter and 2 mm thickness with the boundary perpendicular to the circular faces. The direction of subsequent diffusion was parallel to $\langle 1\,1\,0\rangle$, i.e. along the tilt axis. The polycrystalline specimen was slightly smaller and contained several large grains of approximately 1 to 2 mm diameter. The as-cut specimens were annealed at 1600° C for 40 h in oxygen and then polished to a mirror finish using diamond paste on fibre laps. This polishing step is known to produce a large dislocation density within a depth of a few micrometers below the surface [6]. The polished specimens were then annealed at either 1100° or 1400° C for 16 h in oxygen. (This heat treatment will be referred to as a "dislocation anneal" since its purpose was to reduce the dislocation density.) This annealing was found to have a significant effect on subsequent diffusion behaviour. The specimens were then given a diffusion pre-anneal in oxygen at 1 atm pressure and at the diffusion temperature (700° C) in order to establish the equilibrium defect structure in the near-surface region.

2.2. Diffusion experiments

A ^{63}Ni tracer was applied to the specimens as described previously [18] and then they were given a diffusion anneal at 700° C in oxygen. The penetration profile of tracer into the specimen was determined by radiofrequency sputter-sectioning [19].

The lateral distribution of tracer in the specimen was determined by autoradiography using Kodak AR10 stripping emulsion after exposure for 44 h and 5 min development in Kodak D19.

2.3. Analysis of grain-boundary composition

After the diffusion experiments the bicrystal samples were fractured intergranularly under a bending stress in air at ambient temperature. The purity of the surface and sub-surface material, on the grain boundary facets thus exposed, was studied using scanning electron microscopy (SEM), energy-dispersive X-ray spectroscopy (EDX) and Auger electron spectroscopy (AES).

Several attempts were also made to prepare thin foils in order to examine the grain boundary region by transmission electron microscopy (TEM). These were unsuccessful because the foil always fractured at the boundary during the final stages of preparation.

3. Results

3.1. Tracer penetration profiles

The theoretical solution to the diffusion equation for a combination of lattice and grain boundary diffusion and a 'thin source' surface boundary condition has been given by Suzuoka [20]. In the case of a serial section experiment, the penetration profile may be written as:

$$\bar{C}_s(y, t) = K(\pi Dt)^{-\frac{1}{2}}[\exp(-y^2/4Dt) + \bar{C}_{II}/n] \quad (1)$$

$\bar{C}_s$ is the average concentration at depth y, K is the surface concentration at $t = 0$ and $n = g/(4Dt)^{\frac{1}{2}}$ where g is the grain size. $\bar{C}_{II}$ is a complex function (tabulated by Suzuoka) of several variables and describes the contribution from grain boundary diffusion. Fig. 2 shows the penetration profiles of tracer in bicrystal 1 ($\theta = 39.5$) for the two dislocation-anneal temperatures. (The other specimens gave broadly similar results.) These profiles are similar to those determined in earlier studies using single crystals [6] and have two contributions. The first part, near the surface, is an apparent lattice contribution and the second part, penetrating further, is due to diffusion along low angle boundaries comprising networks of dislocations. This second part is sensitive to specimen pre-treatment. Annealing at 1400° C (as opposed to 1100° C) reduces the concentration in the second part by approximately a factor of 5 and presumably reduces the average dislocation density by the same factor. This is supported by Sears' observations of the influence of annealing on dislocation densities in NiO [21]. The average apparent diffusion coefficient deduced from the first part of all the profiles is approximately $30 \times 10^{-15}\,cm^2\,sec^{-1}$ which is considerably larger than that determined in previous work ($1.2 \times 10^{-15}\,cm^2\,sec^{-1}$ [18]). However, diffusion anneals of 2 h at 700° C are far too short for good lattice diffusion measurements (2 h was chosen as the optimum for observing grain-boundary diffusion) and these high apparent values can have several causes. Consequently a longer diffusion anneal was carried out on the polycrystal specimen. The resulting value of D was $0.5 \times 10^{-15}\,cm^2\,sec^{-1}$. This is considered to be in acceptable aggrement with the earlier results and indicates that lattice diffusion in these specimens is characteristic of pure NiO.

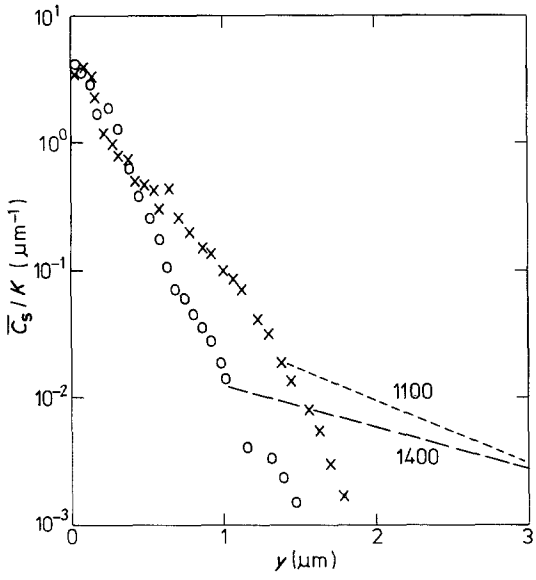

Figure 2 ^{63}Ni tracer penetration profiles in bicrystal 1, $\theta = 39.5°$, after a diffusion anneal of 2 h at 700° C. The individual profiles correspond to dislocation anneals at (x) 1100° and (o) 1400° C. The broken lines are the expected contributions from diffusion along high angle boundaries in a specimen with 10 μm grain size (see text).

The second part of each profile was interpreted as being due to diffusion along low-angle boundaries and was analysed as in earlier work [6] assuming $D = 1.2 \times 10^{-15}\,cm^2\,sec^{-1}$. The resulting values of $D'\delta$ are given in Table I. The average value is $4.8 \times 10^{-19}\,cm^3\,sec^{-1}$ and is in excellent agreement with the earlier measurements ($4.4 \times 10^{-19}\,cm^3\,sec^{-1}$). This confirms that diffusion both in the lattice and along dislocations in the present specimens is consistent with the earlier data and is probably characteristic of pure NiO. In no case is there a detectable contribution to the penetration profile which can be attributed to diffusion along the high angle grain boundaries. This is not surprising because, if we assume that $D'\delta$ in the high angle boundaries is also in agreement with earlier measurements, the high angle boundary contribution is expected to appear at $C_s/K \simeq 10^{-4}\,\mu m^{-1}$ at the very most. This is below the practical limits of detectability (usually between 10^{-4} and $10^{-3}\,\mu m^{-1}$).

3.2. Autoradiography

The depths at which autoradiographs were taken on the three specimens are listed in Table 1. From previous work [3] it was known that nickel diffusion (diffusion anneal 2 h at 700° C), along high angle boundaries in polycrystalline NiO films, is readily detectable by autoradiography at a depth of about 1 μm. The maximum depths at which grain-boundary diffusion was detectable in the present specimens are also given in Table I. The observations may be summarized as follows:

TABLE I Summary of heat treatments and diffusion parameters

Specimen	Dislocation anneal temperature (° C)	Diffusion anneal time (sec)	$D'\delta$ for low angle boundaries ($cm^3 sec^{-1}$)	Depths at which autoradiographs taken (μm)	Extent of diffusion on high angle boundaries
Bicrystal 1 $\theta = 39.5°$	1100	7.2×10^3	7.9×10^{-19}	0.20, 0.41, 0.60, 0.98	Not detectable
	1400	7.2×10^3	3.8×10^{-19}	0.22, 0.50, 0.72, 1.1, 1.6	Not detectable
Bicrystal 2 $\theta = 99.5°$	1100	7.2×10^3	2.6×10^{-19}	0.24, 0.67	Not detectable
	1400	7.2×10^3	2.3×10^{-19}	0.20, 0.62, 1.3, 3.0, 4.1, 5.1, 6.3	Detectable to $\sim 6\,\mu m$
Polycrystal	1100	7.2×10^3	7.7×10^{-19}	0.40, 0.64, 0.90, 1.6, 2.3	Not detectable
	1400	7.2×10^3	2.4×10^{-19}	0.28, 0.56, 0.86	Detectable to $\sim 0.6\,\mu m$
	1400	6.05×10^5	7.1×10^{-19}	—	—

(a) In the polycrystalline specimen, no diffusion along any grain boundary was detectable following the 1100° C dislocation anneal, but was detectable to a depth of 0.6 μm in about half of the boundaries after the 1400° C dislocation anneal. At three-grain junctions, where not all boundaries showed diffusion, the transition from diffusion to no detectable diffusion was very sharp and located at the junction itself.

(b) Bicrystal 1 ($\theta = 39.5°$) showed no evidence for grain-boundary diffusion after either the 1100 or the 1400° C dislocation anneal.

(c) Bicrystal 2 ($\theta = 99.5°$) showed no detectable grain-boundary diffusion after the 1100° C dislocation anneal, but after the 1400° C dislocation anneal grain boundary diffusion was detectable to a depth of approximately 6 μm. A set of autoradiographs of a representative part of this grain boundary, taken at various depths up to 5.1 μm, are shown in Fig. 3. The inhomogeneous nature of diffusion in this boundary is readily apparent.

3.3. Examination of intergranular fracture surfaces

3.3.1. Bicrystal 1, $\theta = 39.5°$

Intergranular failure occurred over approximately one third of the boundary area, after application of very considerable stress. The grain boundary surface showed large-scale faceting (Fig. 4a), with facet edges aligned roughly parallel to the bicrystal growth axis, and a number of faceted intergranular cavities (the origins of which are discussed by Fahri *et al.* [22]). The lack of contrast in the back-scattered electron image

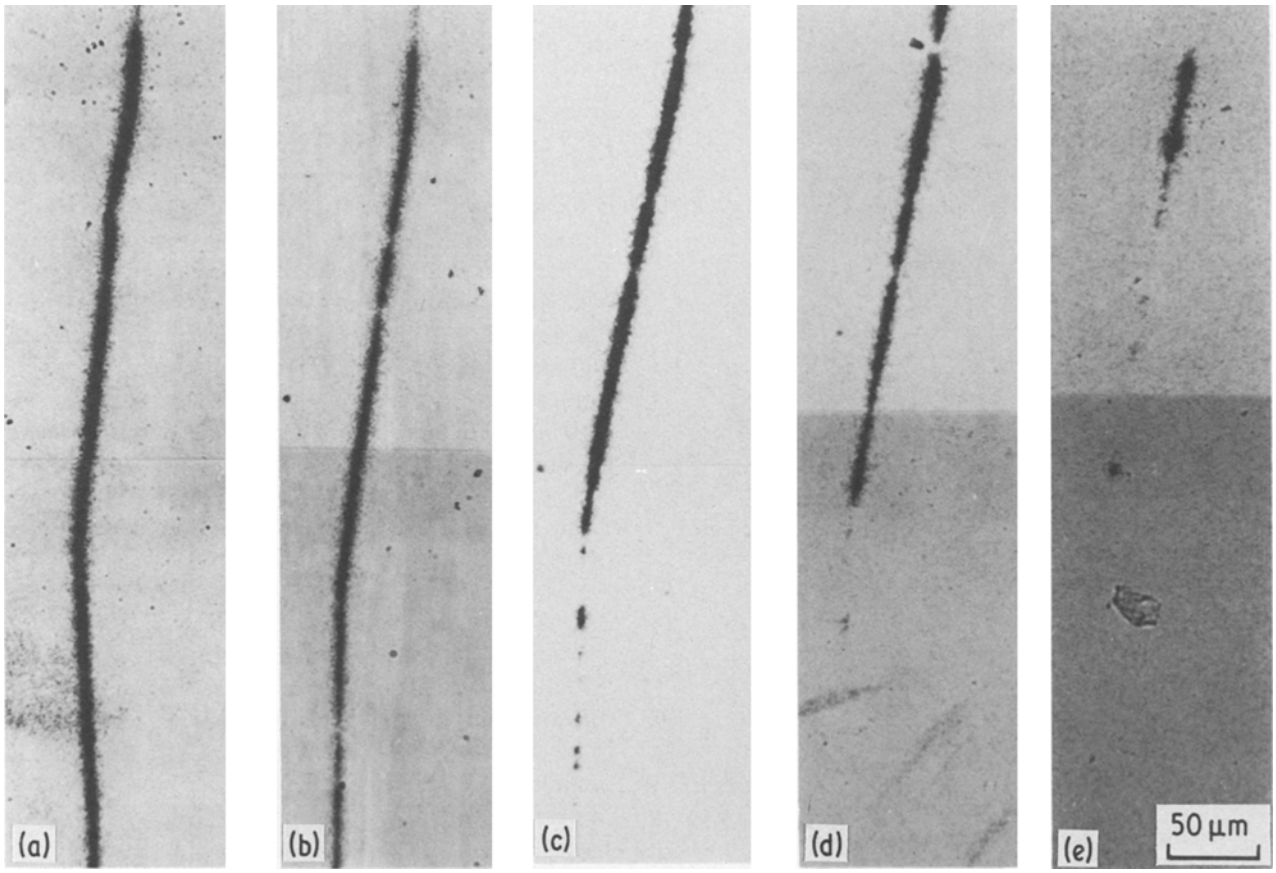

Figure 3 Autoradiographs showing grain boundary diffusion in bicrystal 2, $\theta = 99.5°$, after a dislocation anneal at 1400° C and diffusion anneal at 700° C for 2 h. The labels indicate the depth below the original surface at which the autoradiograph was taken. (a) 0.6 μm, (b) 1.3 μm, (c) 3.0 μm, (d) 4.1 μm, (e) 6.1 μm.

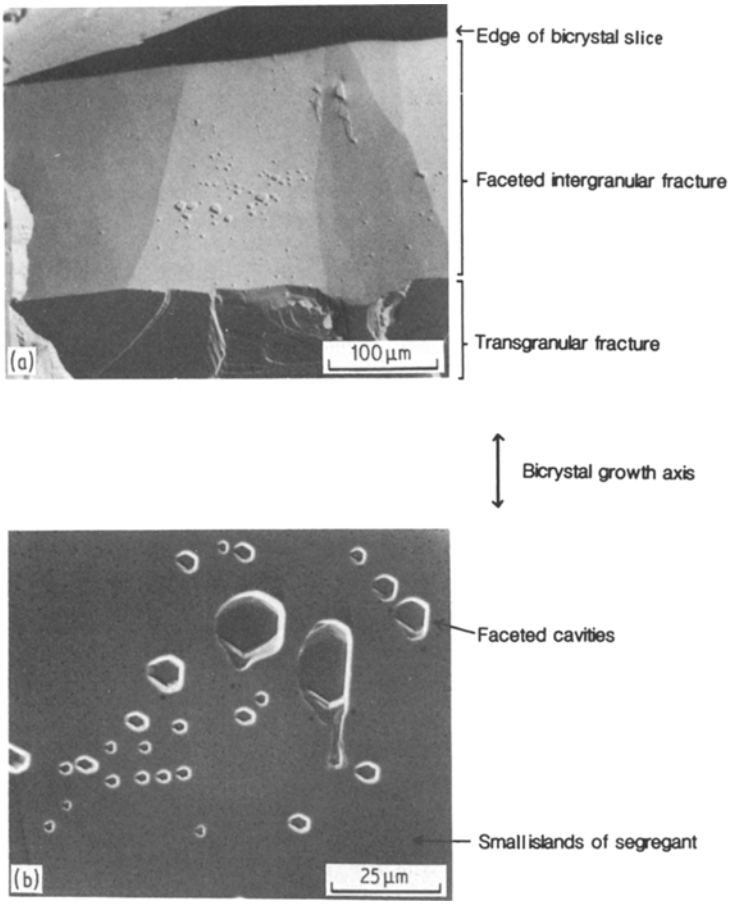

Figure 4 SEM of intergranular fracture surface, bicrystal 1, $\theta = 39.5°$.

(Fig. 4a) indicates the absence of thick second phase particles on the boundary plane. However, secondary electron images (Figs 4b and 5a) reveal a fairly uniform dispersion of some segregated material in the form of dark spots, 0.2 to 1 μm in diameter. These spots appear to accumulate as larger elongated patches along facet edges. In addition, a band of filamentary precipitates was present close to the polished surface of the sample slice (Figs 5a and 7a).

EDX semi-quantitative analysis was carried out at low accelerating voltage to reduce beam penetration into the NiO substrate, and the results are given in Table II. The dark segregant was found to contain silicon, calcium and aluminium (Fig. 5b). Auger analysis maps, shown in Fig. 6, confirmed the presence of calcium and the reduction in nickel and oxygen at these spots. The filamentary second phase was found (Fig. 7) to include potassium, calcium, sodium, sulphur, silicon and chlorine.

3.3.2. Bicrystal 2, $\theta = 99.5°$

This sample fractured easily revealing intergranular facets decorated with large second phase particles. The distribution of particles and of facet edges again appeared to have a general alignment related to the bicrystal growth direction (Fig. 8).

Two major compositional types of boundary precipitates were clearly differentiated by the atomic number-dependent contrast (Fig. 9a). The lighter phase (higher mean Z) contained nickel, calcium, silicon and oxygen as major constituents (Fig. 9b). The darker phase was shown by AES to be essentially nickel-free; combined AES and EDX analysis identified calcium, silicon, sulphur and oxygen as the major

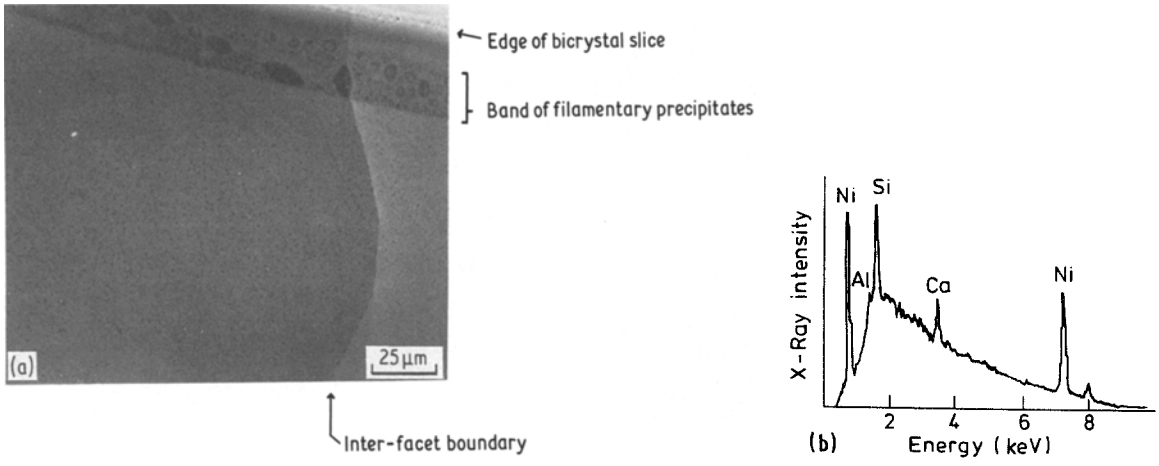

Figure 5 SEM/EDX of islands of segregant, bicrystal 1, $\theta = 39.5°$.

TABLE II Semi-quantitative chemical analysis of intergranular segregants and precipitates (concentrations in relative atomic per cent)

Bicrystal	Phase	Refer to Fig.	Analysis type	Ni	O	Ca	Si	Al	Ba	Na	K	S	Cl	C
1. $\theta = 39.5°$	Filamentary precipitates	7b	AES	12.1	13.6	9.4	1.8				26.6	7.5	7.0	22.0
	Rounded segregant spots	5b	EDX	45.0		9.0	39.8	6.2						
2. $\theta = 99.5°$	Dark phase (low $\bar{Z}$)	9c	EDX	2.5		55.0	38.0	2.4			0.8		1.3	
		10a	AES		50.3	38.3	4.7					6.8		
	Light phase (high $\bar{Z}$)	9b	EDX	37.5		29.4	23.3				2.8		7.1	
Unknown	Rounded phase	11b	AES		24.5	6.1	10.7		32.8					26.0
	Grain boundary	11c	AES	41.4	19.6									39.0

Notes: (a) AES quantification by cubic polynomial smoothing, successive channel differentiation and weighting of peak heights by elemental sensitivity factors.
(b) EDX quantification by determining peak areas and applying ZAF correction (standardless analysis).
(c) Accuracy quoted above is not justified by the data and quantification procedures.
(d) AES data for C represent surface contamination.

elements in these precipitates (Figs 10a, 9c). In addition, Auger depth profiling (Fig. 10b) of this darker phase demonstrated the considerable thickness of the intergranular precipitates (up to a few hundred nm).

3.3.3. Miscellaneous bicrystals

Other bicrystals manufactured by the same technique, but less well characterized crystallographically than the above samples, were also studied. The intergranular facets of one such specimen were decorated with rounded and elongated particles consisting of barium, silicon, calcium and oxygen (Fig. 11b). The patches of NiO between these particles were essentially free of segregation (Fig. 11c).

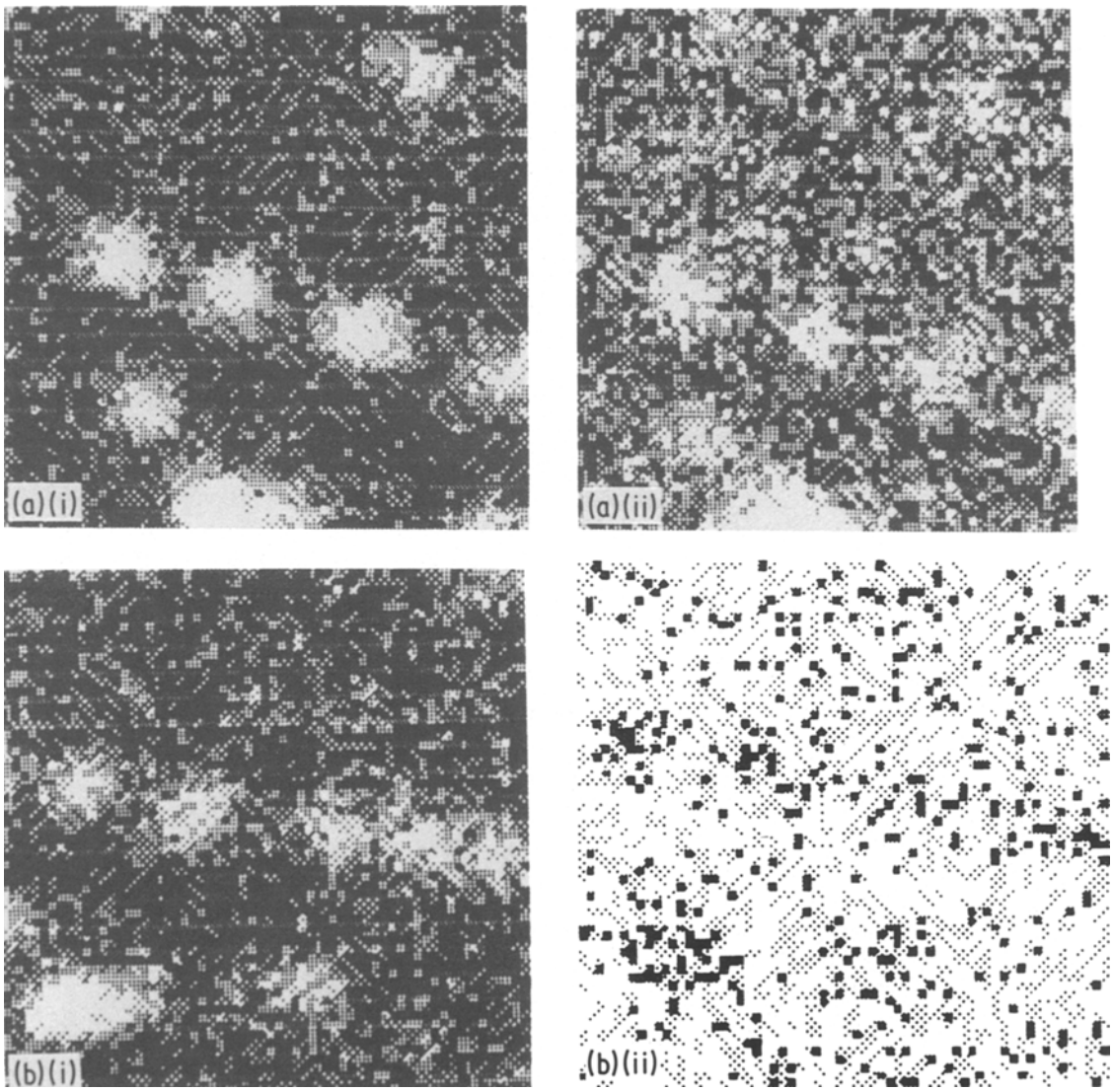

Figure 6 Auger maps of islands of segregant, bicrystal 1, $\theta = 39.5°$: (peak-background)/(background)data, with dark shading representing high concentrations. Each field of view 10 μm × 10 μm. (a) (i) nickel, (ii) oxygen. (b) After sample drift (i) nickel, (ii) calcium.

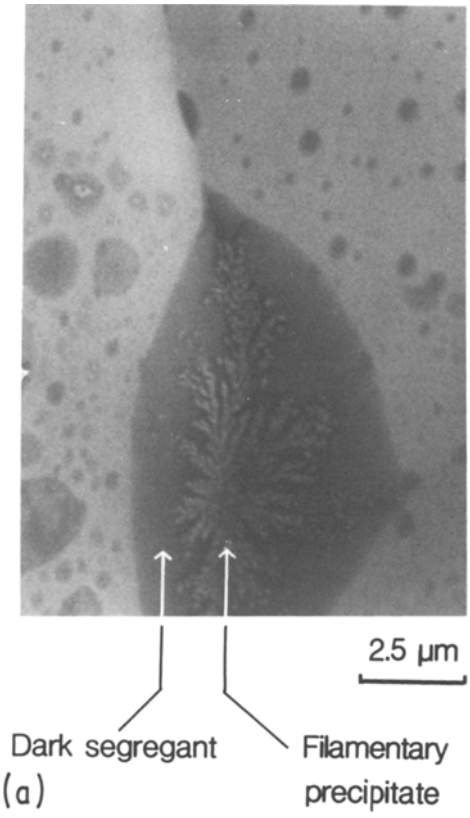

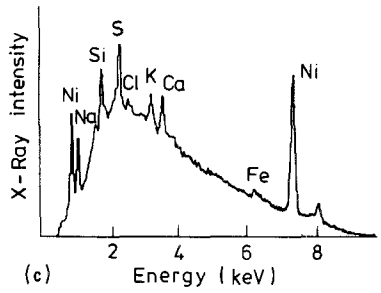

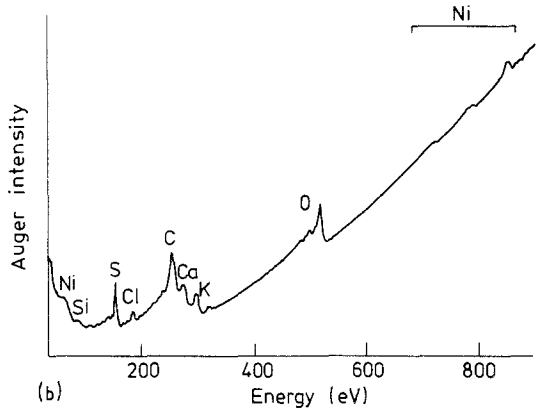

Figure 7 SEM/AES/EDX of filamentary precipitate, bicrystal 1, $\theta = 39.5°$.

4. Discussion

The analysis of nickel tracer diffusion profiles in the current experiments gives results for lattice diffusion and diffusion along low angle boundaries (dislocation arrays and networks) which are in acceptable agreement with the results of previous work on NiO. There is good evidence, particularly the dependence of diffusion on oxygen activity, that these results are characteristic of the pure, non-stoichiometric oxide. Furthermore, the earlier results of diffusion along high angle grain boundaries in polycrystalline NiO films are also probably characteristic of pure NiO because they also show a similar dependence on oxygen activity and because the values of $D'\delta$ are somewhat greater than those for low angle boundaries (see Fig. 1).

Diffusion along high angle boundaries, in the bicrystal and large-grained polycrystalline specimens, in the experiments described here is not consistent with the earlier observations. In particular, diffusion in the individual boundaries has been shown to be inhomogeneous and sensitive to boundary type and thermal history. In addition, chemical characterization of the bicrystal boundaries has revealed considerable contamination, mainly by calcium and silicon.

4.1. Effect of boundary misorientation

Bicrystals, similar to the ones used in the present work, have been used previously in studies of grain-boundary energy as a function of misorientation about a $\langle 1\,0\,0 \rangle$ tilt axis [23] and $\langle 1\,1\,0 \rangle$ axis [24]. Bicrystal 1($\theta = 39.5°$), in which no diffusion could be detected in the high angle boundary, has a misorientation which is close to a local minimum in experimental results of grain boundary energy as a function of θ(at $\Sigma = 9$, $\theta = 38.9°$). However, both experimental results and theoretical calculations [25] agree that this minimum is only shallow. Therefore, particularly slow diffusion would probably not be expected at this value of θ.

Bicrystal 2($\theta = 99.5°$) is not expected to have a low boundary energy, based on either the experimental data or the theoretical calculations. This boundary was, therefore, also expected to show detectable grain boundary diffusion, but it did so only after the 1400° C dislocation anneal.

The grain misorientations in the large-grained polycrystalline specimen were not controlled. The orientations of several individual grains were determined by electron channelling patterns in SEM. The resulting misorientations could be described as "random high-angle" with no simple orientation relationships between any adjacent grains. Again, therefore, there was no obvious correlation between boundary geometry and whether the boundary showed detectable diffusion, or not.

4.2. Effect of the dislocation anneal

The purpose of the dislocation anneals was to reduce the dislocation density in the near-surface region of the specimen. The lowering of the contribution from dislocations to the tracer penetration profile after a dislocation anneal at 1400° C is consistent with fulfilling this purpose. One possible reason why the 1400° C dislocation anneal enabled grain-boundary diffusion to be detected subsequently, in both bicrystal 2 and the polycrystalline specimen, is that the diffusion kinetics were significantly altered. The lower dislocation density has two effects on diffusion kinetics. First, it reduces the background of diffusion in low angle boundaries and, second, it reduces sideways

Figure 8 SEM of intergranular fracture surface, bicrystal 2, $\theta = 99.5°$.

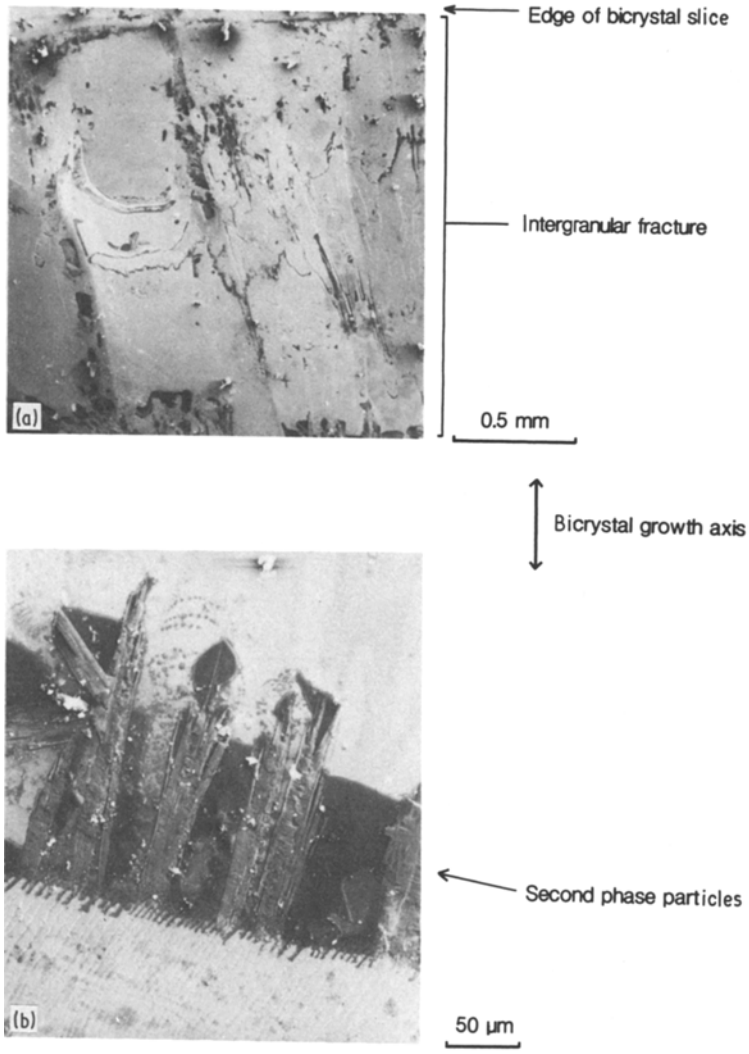

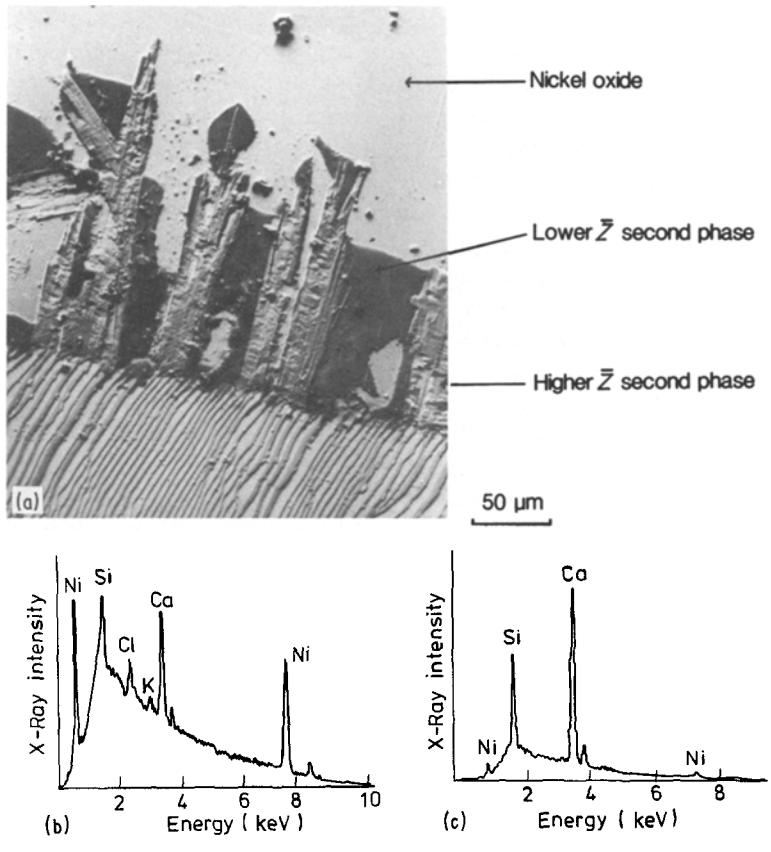

Figure 9 SEM/EDX of second phase particles, bicrystal 2, $\theta = 99.5°$. (a) back-scattered signal; (b) light (high $\bar{Z}$) phase; (c) dark (low $\bar{Z}$) phase.

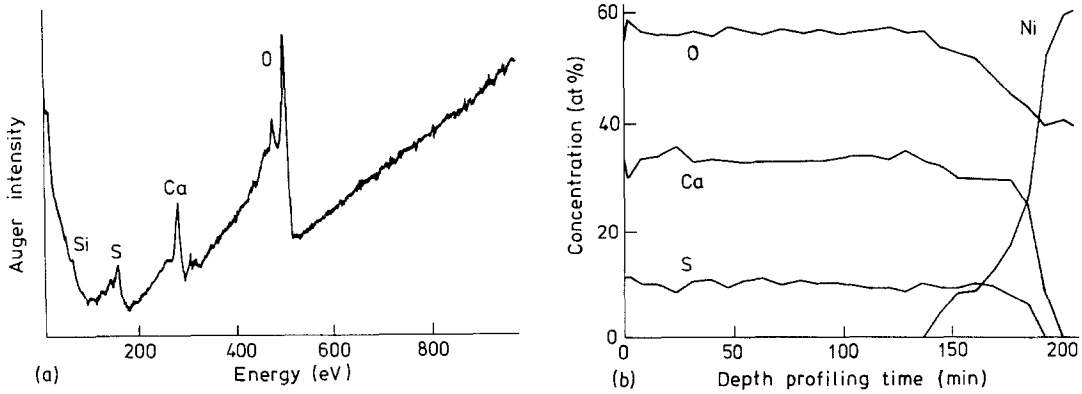

Figure 10 Auger analysis and depth profile of dark (low $\bar{Z}$) phase, bicrystal 2, $\theta = 99.5°$.

diffusion out of the high angle boundary into the crystals. We have tried to assess the likely consequences of these processes on the detectability of grain-boundary diffusion by assuming that the influence of dislocations can be included as an effective lattice diffusion coefficient, D_{eff}, given by the average

$$D_{\text{eff}} = D + \frac{2(D'\delta)_l}{g_l} \qquad (2)$$

Here $(D'\delta)_l$ and g_l are grain-boundary diffusion parameters and grain size for the low angle boundaries. With values of $D = 1.2 \times 10^{-15}\,\text{cm}^2\,\text{sec}^{-1}$, $(D'\delta)_l = 4.8 \times 10^{-19}\,\text{cm}^3\,\text{sec}^{-1}$ and $g_l = 1\,\mu\text{m}$, D_{eff} is predicted to be $10 \times 10^{-15}\,\text{cm}^2\,\text{sec}^{-1}$. (Equation 2 is only strictly valid when $(Dt)^{1/2} \gg g$, but it should serve as an approximate indication of the likely influence of dislocations). This value will be typical of crystals annealed at 1100° C since g_l is known to be about 1 μm in such a case [6]. Since the anneal at 1400° C reduces the low angle boundary contribution by a factor of five, $D_{\text{eff}} = 2 \times 10^{-15}\,\text{cm}^2\,\text{sec}^{-1}$ was assumed to be typical of such material. The expected contribution from the high angle boundaries was computed from Suzuoka's solution assuming $D'\delta = 2.1 \times 10^{-17}\,\text{cm}^3\,\text{sec}^{-1}$ (i.e. as previously measured) for the high angle boundaries and a grain size of 10 μm. Since the lateral resolution of the autoradiography is a few micrometers, this gives a reasonable guide to detectability. The calculated contributions (now to the autoradiograph from within 5 μm of the boundary, rather than to the total penetration profile) are shown as broken lines in Fig. 2. Detectability may be assessed by the value of C_s/K at which there is an order of magnitude difference between the background of dislocation diffusion and the high angle boundary contribution. The estimates demonstrate that this $(C_s/K \sim 10^{-3}\,\mu\text{m}^{-1})$ is not very sensititve to the dislocation content. We therefore conclude that the influence of the dislocation anneal on the detectability of high angle boundary diffusion is not due to the effect of dislocations on diffusion kinetics.

There are many possible effects that the dislocation anneal may have had, in addition to reducing the dislocation content. For example, the intersection between the boundary and the surface was grooved to a depth of up to 1 μm after annealing at 1400° C. Since

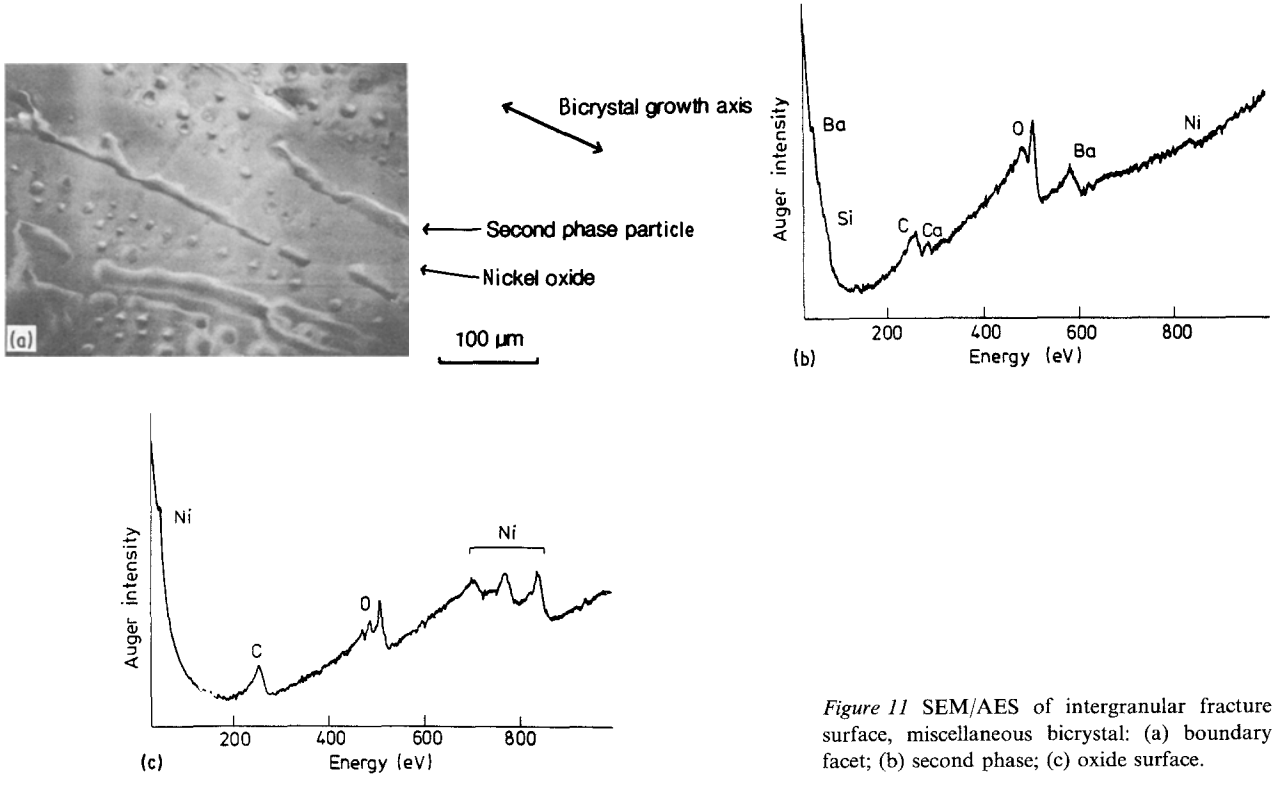

Figure 11 SEM/AES of intergranular fracture surface, miscellaneous bicrystal: (a) boundary facet; (b) second phase; (c) oxide surface.

the tracer was deposited on the grooved surface, the deeper grooves could result in apparent grain boundary penetration. However, qualitative examination of individual boundaries in the polycrystalline specimen showed that there was no correlation between depth of grooving and grain boundary diffusion. It therefore seems likely that the dislocation anneal has actually altered the boundaries themselves in some way (e.g. by a redistribution of impurities).

4.3. Influence of impurities

Characterization of the NiO bicrystal grain boundaries used in the present studies revealed considerable contamination of the boundaries by calcium and silicon oxides, especially in bicrystal 2. (The characterization of samples is representative of their state after all the diffusion experiments had been completed and is therefore the result of a complex thermal history.) It has been estabilished that, in metals, segregation of impurities to grain boundaries can have a profound effect on grain boundary diffusion [26]. In some cases the diffusion coefficient is increased by the segregant, in some cases decreased and in others either increased or decreased, depending upon concentration. There is no obvious way of predicting whether the segregation and second phase precipitation observed in the present boundaries is likely to promote or suppress diffusion along the boundary. Nevertheless, the inhomogeneous nature of diffusion in these boundaries and the sensitivity to heat treatement strongly suggests that it is the distribution of impurities at the boundary which controls the extent of grain boundary diffusion in all these specimens.

We can propose a speculative rationalization of the present observations as follows. When the calcium and silicon impurities are dilute, or well-dispersed, in the boundary they are distributed as in bicrystal 1. They will be present as a thin film, or islands, of amorphous material, and will probably block diffusion along the boundary. At higher concentrations, and after some heat-treatment, the distribution of impurities will be as in bicrystal 2; as thicker films of crystalline material. These may promote diffusion along the boundary at the incoherent interfaces between the impurity phase and the NiO matrix, if the boundary phase forms a continuous pathway.

It is likely that impurities have been significant in all the previous work which has been attempted using bicrystal specimens of oxides. This is also believed to be the case in the alkali halides [27]. The reason for this depressing sitution seems to be that impurities which are essentially insoluble in the matrix will segregate strongly to surfaces and grain boundaries. In a bicrystal specimen, the total grain boundary area is so small in comparison with the volume of the specimen that even a low level of matrix impurity can result in heavy contamination of the boundary. In fine-grained polycrystalline material this problem is reduced in proportion to the total grain boundary area (often a factor of $\sim 10^3$).

This raises some doubts about whether previous work on NiO boundaries can be interpreted as being characteristic of "clean" boundaries. There is obviously no substitute for a detailed structural and chemical characterization of the actual boundaries which are used in measurements of other properties, such as energy or diffusivity, but this has not been done in the past. The grain-boundary energy measurements of Dhalenne *et al.* [23, 24] were made on bicrystals prepared from the same boules as those examined here. The grain-boundary energy data do not give any indication of a significant influence of impurities (e.g. large variability), whereas the bicrystals examined here do show significant contamination. It is possible that the boundary energy experiments are not sensitive to impurities (e.g. because the contaminants at the intersection of the boundary with the surface are lost by evaporation) or that the bicrystals which were used in the energy studies did not have such heavily contaminated boundaries as those examined here. Rühle and Sass [28] have examined, by TEM, grain boundaries in large-grained polycrystalline specimens, fabricated in another laboratory by a similar method. They found no sign of heavy contamination (such as that in bicrystal 2) of their boundaries. However, one possible explanation of their experimental observations is that an impurity is segregated at the boundary core [29]. The grain-boundary diffusion data of Atkinson and Taylor [3, 16] could also have been influenced by impurity segregation, although TEM characterization showed no gross contamination and other observations mentioned previously suggest that impurity segregation was not significant. Attempts to examine the boundaries in those thin polycrystalline films by surface analytical techniques have been unsuccessful.

In the absence of direct evidence to the contrary, it is likely that these earlier data for both boundary energy and diffusion are characteristic of pure NiO. Nevertheless, the importance of structural and chemical studies on the same boundaries used for the measurement of other boundary properties is clearly demonstrated if reliable links between boundary structure and these properties are to be established.

Acknowledgement

We wish to thank Professor A. Revcolevschi and Mme F. Barbier for providing specimens.

References

1. A. ATKINSON, R. I. TAYLOR and A. E. HUGHES, *Phil. Mag. A* **45** (1982) 823.
2. A. ATKINSON, *Solid State Ionics* **12** (1984) 309.
3. A. ATKINSON and R. I. TAYLOR, *Phil. Mag. A* **43** (1981) 979.
4. M. L. VOLPE and J. REDDY, *J. Chem. Phys.* **53** (1970) 1117.
5. W. K. CHEN and N. L. PETERSON, *J. Phys. Chem. Solids* **33** (1972) 881.
6. A. ATKINSON and R. I. TAYLOR, *Phil. Mag. A* **39** (1979) 581.
7. T. KWOK, P. S. HO, S. YIP, R. W. BALLUFFI, P. D. BRISTOWE and A. BROKMAN, *Phys. Rev. Lett.* **47** (1981) 1148.
8. D. M. DUFFY and P. W. TASKER, *J. Phys. (Paris) Coll. C4* **46** (1985) 185.
9. J. T. ROBINSON and N. L. PETERSON, *Surf. Sci.* **31** (1972) 586.
10. A. ATKINSON, *J. Phys. (Paris) Coll. C4* **46** (1985) 379.
11. B. J. WUENSCH and T. VASILOS, *J. Amer. Ceram.*

Soc. **47** (1964) 63.
12. D. R. McKENZIE, A. W. STEARCY, J. B. HOLT and R. H. CONDIT, *ibid.* **54** (1971) 188.
13. J. W. OSENBACH and V. S. STUBICAN, *ibid.* **66** (1983) 191.
14. K. HIROTA and W. KOMATSU, *ibid.* **60** (1977) 105.
15. W. K. CHEN and N. L. PETERSON, *ibid.* **63** (1980) 566.
16. A. ATKINSON and R. I. TAYLOR, *Phil. Mag. A* **45** (1982) 583.
17. A. REVCOLEVSCHI, F. BARBIER and M. DECHAMPS, "Physical Chemistry of the Solid State: Applications to Metals and their Compounds", edited by P. Lacombe (Elsevier, Amsterdam, 1984) p. 141.
18. A. ATKINSON and R. I. TAYLOR, *J. Mater. Sci.* **13** (1978) 427.
19. *Idem, Thin Solid Films* **46** (1977) 291.
20. T. SUZUOKA, *J. Phys. Soc. (Jpn.)* **19** (1964) 839.
21. J. S. SEARS, *J. Mater. Sci.* **13** (1978) 2455.
22. R. FAHRI, G. PETOT-ERVAS, C. PETOT, G. DHALENNE and F. LEGUERN, *J. Solid State Chem.* **41** (1982) 147.
23. G. DHALENNE, A. REVCOLECSCHI and A. GERVAIS, *Phys. Status Solidi (a)* **56** (1979) 267.
24. G. DHALENNE, M. DECHAMPS and A. REVCOLEVSCHI, *J. Amer. Ceram. Soc.* **65** (1982) C-11.
25. D. M. DUFFY and P. W. TASKER, *Phil. Mag. A* **48** (1983) 155.
26. F. CABABNÉ-BROUTY and J. BERNARDINI, *J. Phys. (Paris) Coll. C6* **43** (1982) 163.
27. L. B. HARRIS, *J. Phys. (Paris) Coll. C6* **41** (1980) 285.
28. M. RÜHLE and S. L. SASS, *Phil. Mag. A* **49** (1984) 759.
29. M. RÜHLE and W. MADER, "Basic Properties of Binary Oxides", edited by A. Dominguez-Rodriguez, J. Castaing and R. Marques (University of Seville, 1984) p. 297.
30. C. DUBOIS, C. MONTY and J. PHILIBERT, *Phil. Mag. A,* **46** (1982) 419.

Received 27 June
and accepted 10 July 1985